Volume 17, Number 3, 2024. pp. 331-340

Jordan Journal of Physics

ARTICLE

First-principles Study on Structural and Electronic Properties: The Li Based of Full-Hesulter Alloys $LiGa_2Ir$

A. Ouahdani, R. Takassa, F. Elfatouaki, O. Farkad, S. Hassine,
A. El Mouncharih, O.Choukri, E.A. Ibnouelghazi and **D. Abouelaoualim**

LaMEE, Department of Physics, Faculty of Sciences Semlalia, Cadi Ayyad University, P.O. Box 2390, 40000 Marrakech, Morocco.

Doi: **https://doi.org/10.47011/17.3.8**

Received on: 24/09/2022; Accepted on: 17/01/2023

Abstract: Due to their excellent electronic properties, full-Heusler compounds have become one of the most interesting families of alloys in superconductivity. More recently, computational methods have been actively employed to support the rapid discovery of new complete Heusler alloys by identifying stable compositions with desired properties. Therefore, we investigated the stability, structure, and electronic properties of the lithium-based Heusler compound $LiGa_2Ir$ using first-principles calculations. We explored the effects of exchange-correlation, namely Perdew-Burke-Ernzerhof (PBE), PBE+U, and Tran-Blaha modified Becke-Johnson potentials, as well as the effect of heavy metal spin-orbit coupling on these Heusler compounds. The results show that $LiGa_2Ir$ is energetically stable, and the obtained lattice parameter value (a = 6.0927 Å) agrees with the experimental results. $LiGa_2Ir$ exhibits metallic behavior under all three exchange-correlation estimates. A much stronger spin-orbit coupling effect is observed for electronic states with energies below the Fermi level E_F, especially in the Tran-Blaha modified Becke-Johnson approximation. Significant spin-orbit coupling effects are evident from the total and partial density of states figures, especially in the energy range from -4.5 eV to -2 eV. The contributions from Ir-d and Ga-p orbitals are the largest, while the contribution from the Li atom is small. Our findings will benefit future theoretical and practical work on lithium-based full-Heusler alloys.

Keywords: Full-Heusler, DFT, Spin-orbit coupling, Electronic properties, Density of states.

1. Introduction

Heusler alloys have received significant attention due to their attractive physical properties [1] such as interesting magnetic properties [2, 3], high spin polarization [4], spin-gapless semiconducting nature [5], superconductivity [6], diverse optoelectronic [7] and thermoelectric properties [8]. They are considered among the most promising nanomaterials for applications that include thermoelectric materials [9], new spintronic devices [10-13], optoelectronic [14], ferromagnets [15], magnetocaloric materials [16], topological insulators [17], superconductors [6], shape memory alloys [18], and more recently, catalysts [19].

Heusler compounds are among the best intermetallic compounds. They are represented by the general formula X2YZ, XYZ, or XX′YZ, where X, X′, and Y are transition metal atoms and Z is a main group element. Depending on the configuration and number of elements involved, the compounds can be full, half, inverse, semi, or quaternary Heusler alloys. All Heusler compounds crystallize in the L21 cubic

Corresponding Author: D. Abouelaoualim **Email**: dr.abouelaoualim@uca.ac.ma

structure (space group Fm-3m), with four interpenetrating face-centered cubic (fcc) structures [20].

Identifying Heusler materials with interesting physical properties has proven to be a difficult task in scientific research. Among these Heusler compounds, Li-based Heusler materials are gaining increasing attention due to their extraordinary properties and potential applications, particularly in optical and photonic devices, semiconductors for high-efficiency power electronics, and superconductors [14].

Damewood *et al.* investigated the role of Li in half-Heusler LiMnZ (where Z = N, P, Si) in stabilizing and increasing the magnetic moments of half-metals [21]. LiMgBi, LiZnP, LiCdP, and LiAlSi were studied using first-principles density functional calculations by Kandpal *et al.* [22]. This report focused on the examination of band gaps and the nature (covalent or ionic) of bonding in semiconducting half-Heusler compounds [22].

Amudhavalli *et al.* also employed first-principles calculations based on density functional theory to study semiconducting Li-based half-Heusler compounds (LiBeAs, LiBeSb, LiBeBi, and LiScGe) [14]. Their computed electronic structure profile reveals the semiconducting behavior of these materials [14].

Manoj *et al.* studied the thermoelectric properties of Li-based half-Heusler alloys LiYZ (Y = Be, MgZn, Cd and Z = N, P, As, Sb, Bi), showing that all the compounds have larger values of power factors [23].

Weibo Yao *et al.* reported using first-principle predictions of the half-metallic ferrimagnetism in Li-based full-Heusler alloys Mn_2LiZ (Z = Sb, As) with highly ordered structure [24].

The structural, electronic, magnetic, and thermoelectric properties of the new full-Heusler compounds Mn_2LiZ (Z = Si, Ge, and Sn) were investigated by Hadji *et al.*, who showed that these compounds exhibit half-metallic ferrimagnetism with a fairly large gap and a low net spin magnetic moment [25].

The superconductivity in $LiGa_2Rh$ was studied experimentally by Carnicom *et al.*, and it was demonstrated that the full-Heusler compound $LiGa_2Rh$ is a superconductor with a Tc of 2.4K [26].

Using first-principles calculations, Hadji *et al.* reported the structural, electronic, magnetic, and electronic transport properties of new Heusler compounds Mn_2LiZ with Z = Al and Ga [27]. Their findings from the band structure calculations indicated that the Mn_2LiAl compound is a spin-gapless semiconductor and Mn_2LiGa is a nearly spin-semimetal [27].

More recently, Karolina *et al.* studied experimentally and theoretically the superconductivity in the $LiGa_2Ir$ Heusler-type compound. Their measurements indicated a bulk superconductivity with a Tc of 2.94K. Through first-principles calculations, they examined the electron-phonon interaction and the SOC effect on the electronic structure. The phonon dispersion curve showed the dynamical stability of the compound, while the electronic bands and DOS curves indicated a small effect of SOC near the Fermi energy (E_F).

The efficiency and accuracy of DFT are given by the best choice of exchange-correlation (XC) functionals. In the present work, we applied DFT calculations to study the Heusler-type compound $LiGa_2Ir$ with different XC functionals, namely Perdew-Burke-Ernzerhof (GGA-PBE), the Tran-Blaha modified Becke-Johnson (TBmBJ) exchange potential, and the generalized gradient approximation developed by PBE with Coulomb Potential (PBE + U). These functionals have been found to perform better in calculating the structural and electronic properties of several Heusler-type compounds, although they have not been applied previously to $LiGa_2Ir$ examined in the present paper.

We carried out systematic calculations using these XC functionals, combined with SOC effects, to analyze the thermodynamic stability, as well as structural and electronic properties of the $LiGa_2Ir$ Heusler-type compound. This work is structured as follows. Section 2 describes how to calculate. Section 3 presents the results and the discussion on stability, structural properties, and the effects of XC and SOC on the electronic band structure, along with total and partial density of states (DOS and PDOS) profiles. Finally, Section 4 presents the conclusion.

2. Computational Method

We performed calculations in the context of density functional theory (DFT) using the full-potential linearized enhanced plane wave method

(FP-LAPW) implemented in the Wien2k code [28] to characterize the structural and electrical features of the LiGa$_2$Ir Heusler compound. To approximate the XC energy function, we added the PBE form to the GGA, the exchange potential TB-mBJ, and the Coulomb potential to be used (PBE + U). The Hubbard effective potential U_{eff} = U - J (where U represents the Coulomb interaction and J expresses the exchange interaction for both Ir and Ga atoms) was used for strongly d- or f-correlated electrons [29]. In this work, we used an effective U_{eff}= 1.6 eV on the Ir atom site (strongly 5d correlated electrons), computed using the constrained random-phase approximation (cRPA) [30], which yields a very good account of the ground-state electronic and magnetic properties [31-33]. For different approximations of the XC, we performed the calculations in the presence and absence of SOC.

The LiGa$_2$Ir compound consists of three atoms with electronic valence configurations as follows: Ir ($4f^{14}$, $5d^7$, $6s^2$), Ga ($4s^2$, $3d^{10}$, $4p^1$), and Li ($2s^1$). The cutoff energy separating the core and valence states was set at -6 Ry. The muffin-tin (MT) radii used for Li, Ga, and Ir were 2, 2.24, and 2.47 a.u, respectively. The crystal structure was relaxed until the force on each atom converged to less than 0.01 Ry/u.a. We expanded the basis function to R_{MT}xK_{max} = 7, where R_{MT} is the minimum radius of the atomic sphere and K_{max} is the largest k-vector in the plane wave expansion. The charge density of the Fourier expansion was truncated at G_{max}= $12R_y^{1/2}$. The maximum angular momentum of the atomic orbital basis functions was set to l_{max} = 10. The total number of k-points in the first Brillouin zone (BZ) was determined to equal 1000. The iteration process was stopped when the total energy convergence threshold of 0,0001 R_Y was reached.

3. Numerical Results and Discussion

3.1. Structural Properties and Stability

The compound LiGa$_2$Ir crystallizes in a face-centered cubic structure with space group Fm-3m (No. 225). It has the formula unit in the primitive Bravais cell, with atoms occupying the following Wyckoff positions: Li at (4b) (1/2, 1/2, 1/2), Ga (8c) (1/4, 1/4, 1/4), and Ir (4a) (0,0,0). The crystal structure of LiGa$_2$Ir is shown in Fig. 1. The unit cell volume of LiGa$_2$Ir has been optimized.

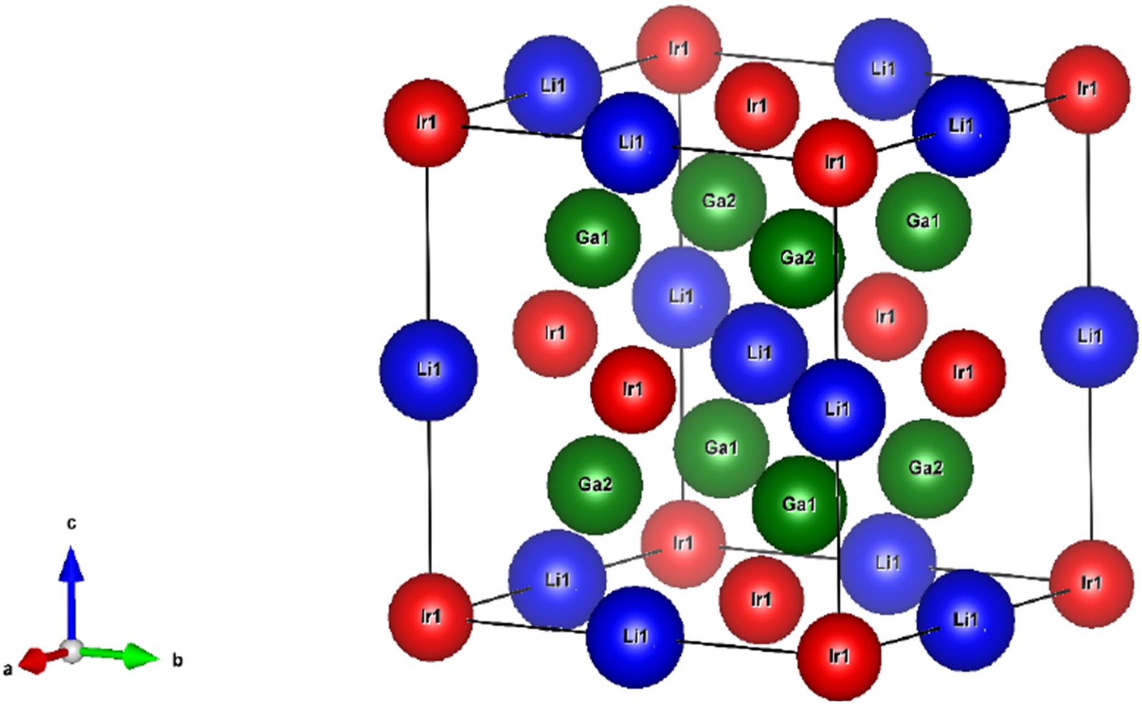

FIG. 1. Optimized crystal structures of LiGa$_2$Ir Heusler alloy compounds.

To assess the stability and ground-state properties of the LiGa$_2$Ir structure, we plotted the variation in unit cell volume as a function of total energy using the Murnaghan equation of state [35], given by:

1. Ref. [34] Experimental value.
2. Ref. [34] GGA-PBEsol without SOC.
3. Ref. [34] GGA-PBEsol with SOC.
4. Ref. [26] Other theoretical methods.

$$E(V) = E_0 + \left[\frac{B_0 V}{B_0'} \left(\frac{(V_0/V)^{B_0'}}{B_0' - 1} + 1 \right) - \frac{B_0 V}{B_0' - 1} \right] \frac{1}{14703.6} \quad (1) \; (1)$$

where E_0 is the minimum energy at 0 K, V is the unit cell volume, V_0 is the unit cell volume at P = 0 GPa, B_0 is the bulk modulus, and B_0' is the pressure derivative of the bulk modulus.

The total energy (E) versus volume (V) for the $LiGa_2Ir$ structure is plotted in Fig. 2. The equilibrium geometry is established by minimizing the energy E(V) as a function of volume using the GGA-PBE approximations, where the optimized volume is the volume corresponding to the minimum of the E(V) curve. On the other hand, the ground-state energy of the unit cell, corresponding to the optimized lattice parameter, is the energy obtained as the minimum energy. Table 1 shows the estimated ground-state parameters, with a lattice constant value of a = 6.0927Å, which is in good agreement with previous theoretical and experimental data [34]. In addition, the table shows the results of another Li-based full-Heusler compound, $LiGa_2Rh$, indicating that the lattice constant of $LiGa_2Rh$ is a little lower than that of $LiGa_2Ir$, which may be due to the larger size of Ir atoms compared to Rh.

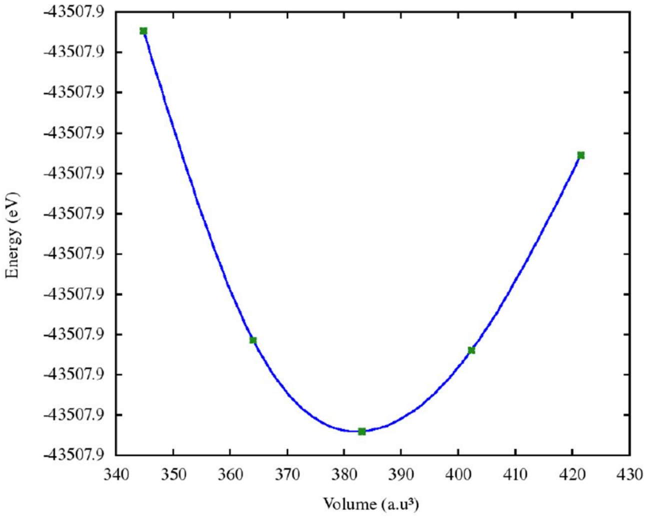

FIG. 2. Optimized energy-volume curves of $LiGa_2Ir$ Heusler alloy compounds under the PBE-GGA exchange-correlation function.

TABLE 1. The calculated values of lattice constant (a), unit cell volume at $P = 0\ GP_a$ (V_0), bulk modulus (B_0), pressure derivative of bulk modulus (B_0'), minimum total energy (E_0), and band gap (E_g) for $LiGa_2Ir$ Heusler alloy compound.

	V_{xc}	a (Å)	V_0 (Å^3)	B_0 (GPa)	B_0' (GPa)	E_0 (Ry)	E_g (eV)
$LiGa_2Ir$ (This work)	PBE	6.0927	381.57	123.191	5.2317	-43507.937	0
	PBE+ SOC						0
	PBE+U						0
	PBE+U +SOC						0
	TB-mBJ						0
	TB-mBJ+ SOC						0
	Other	6.0322 [1]	-	-	-	-	0 [2]
		6.0161 [2]	-	-	-	-	0 [3]
		6.0164 [3]	-	-	-	-	
$LiGa_2Rh$		5.9997 [4]	215.97 [4]				0 [4]

To investigate the stability and the possibility of synthesis of the $LiGa_2Ir$ compound, we calculated the formation energy using Eq. (2) [36, 37]:

$$E_f = \frac{E_{tot}\left(LiGa_2Ir\right) - \mu_{Li} - 2\mu_{Ga} - \mu_{Ir}}{4} \quad \textbf{(2)}$$

where $E_{tot}(LiG_{a2}Ir)$ is the total energy of the $LiGa_2Ir$ compound, while μ_{Li}, μ_{Ga}, and μ_{Ir} are the chemical potentials for Li, Ga, and Ir atoms, respectively. These chemical potentials are calculated as the total energy per atom of the most stable structure of the elements. The bulk forms of these atoms are considered the most stable structures. A negative calculated formation energy (E_f = -0.65 eV) indicates that the $LiGa_2Ir$ compound is structurally stable and experimentally synthesizable [38, 39, 11].

3.2. Electronic properties

3.2.1 Exchange-correlation Effects on the Electronic Band Structure

The generalized gradient approximation PBE and PBE+U are used to treat the potential exchange-correlation function, where U is the Hubbard site [40]. A Coulomb interaction correction of U = 0.50 eV was employed in this work for transition metal Ir. Due to the confined 3d or 4f orbitals of transition metal atom Ir in Heuslers, the GGA+U method on Coulomb repulsion may provide important benefits.

Additionally, we used the TB-mBJ approximation, where the combination coefficient is set in the mBJ potential according to the electron density distribution of each system under study (mBJ) [41]. The mBJ, which is a part of the Kohn-Sham (KS) DFT, is a semilocal technique with a low computational cost that can create KS band gaps that are more consistent with experimental bands than conventional GGA functionals [41, 42].

This section contains the calculation of the band structure of the $LiGa_2Ir$ compound along the highly symmetrical directions of the first Brillouin zone, specifically the *W-L-Γ-X-W-K* path, as shown in Fig. 3. In addition, we detail how the band structure and band gap are affected by the XC functionals and the SOC effect.

Using PBE, PBE+U, and TB-mBJ, we notice that all three approaches exhibit similar behavior. For the most part, a few valence bands touching the Fermi level can be seen clearly lying to a metallic.

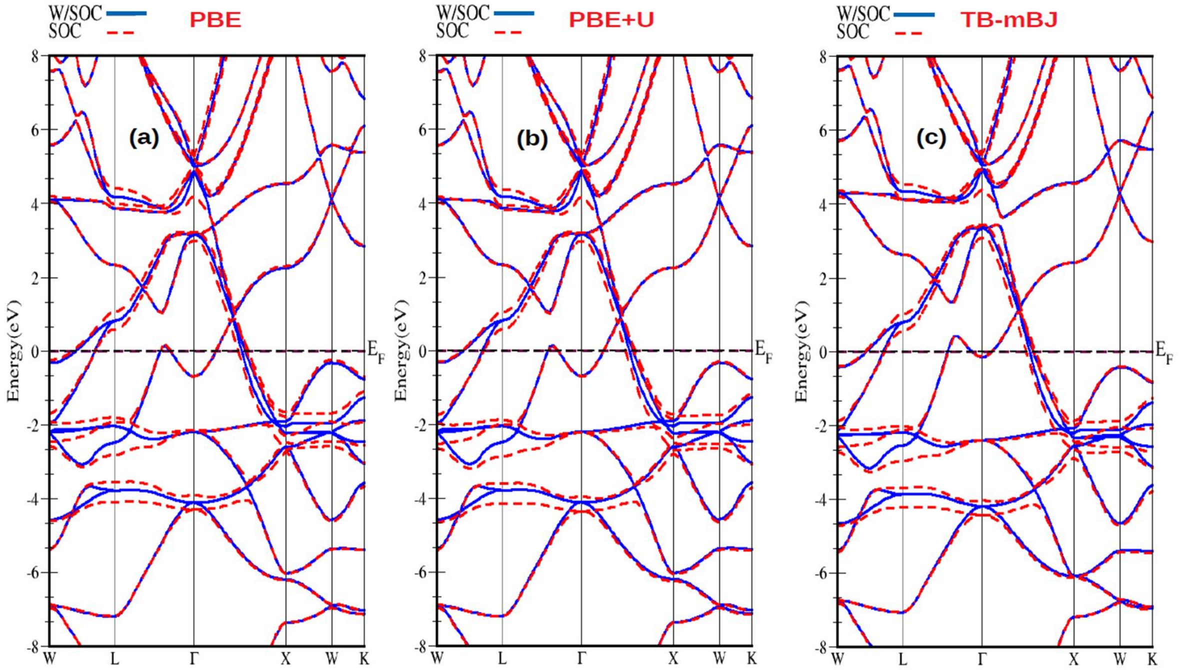

FIG. 3. Calculated band structures without (blue lines) and with (red lines) SOC for *$LiGa_2Ir$* using PBE, PBE + U, and TB-mBJ XC approximations.

In Fig. 3(a), we present the calculated band structure with GGA-PBE approximation, which denotes metallic character in the region where the Fermi level crosses the energy valence bands. Although U is used, the electronic band structure of PBE+U is still quite similar to those of PBE, as seen in Fig. 3(b). However, the band structures under TB-mBJ, depicted in Fig.3(c), are slightly different. We may observe that the bands separate along the X direction, especially at energies below 7 eV, while the bands move toward one another along the G direction in the conduction band. The mBJ causes the valence bands to shift upward, placing the Ef within the valence band. Under all three XC estimates, *$LiGa_2Ir$* exhibited metallic behavior.

3.2.2 SOC Effects on the Band Structure

The spin-orbit coupling (SOC) effect plays a crucial role in compounds containing heavy elements like Iridium (Ir), as it significantly impacts the electronic properties. SOC increases the kinetic energy of electrons and the relativistic effects become very important. Furthermore, SOC interactions were taken into account in this study to enhance the XC approximation calculations of our material [43].

To better understand the application of first-principles approaches, we need to clarify the physical basis for the observed behavior of $LiGa_2Ir$. The band structures of $LiGa_2Ir$ obtained by PBE, PBE+U, and TB-mBJ with and without SOC are plotted with blue and red lines, respectively, and are shown in Fig. 3. The lower and upper part of the valence band consists of the Ir-5d, Ga-4s, and Ga-4p states (about 10 eV), while the lower part of the conduction band consists of Ga-4s and I-p states. The contribution from Li is negligible, as detailed in the DOS section. From the band structure obtained by the TB-mBJ method, it can be seen that the Ir-5d states move to higher energy levels, and a blurring along VB leads to passing the Fermi level. The Fermi level was set as 0 eV. The constituent atoms of the compound are not particularly heavy, so spin-orbit coupling has no visible effect on the electronic states near the Fermi level [42]. However, for electronic states with energies below Ef, we observe much stronger SOC effects, such as band anticrossing in the W-Γ direction. Therefore, upon further analysis, three bands cross the Fermi level. So, it is clear that most of the bands in the XC approximation used in this study are metallic.

All atomic sites in the cubic structure of $LiGa_2Ir$ have T_d symmetry, which causes the crystal field to split the d-orbitals of Ir atoms into degenerate double and triple orbitals, E(dx2-y2, dz2) and T2 (dxy, dyz, dzx), respectively [44-46]. The p-orbitals reside in the T2 state, resulting in a triplet which the SOC then produces. This is the nearest neighbor for our structures, and the d-states with the same T2 or E symmetry hybridize with each other.

The SOC in the X-W-K direction has no significant impact on the degeneracy of the CBM bands. The point-occupied state is VBM, which is a degenerate triplet (T2) in the absence of SOC, as shown in Fig.3. XC and SOC have a similar effect for each of the three estimates. The states with the highest and lowest occupancy rates are adjusted up and down to maintain balance. However, the most and least occupied states are moved up and down for W-L-Γ-X, respectively. In the following subsection, we will delve into the details of our findings by combining the total and partial density of states (DOS and PDOS) computations.

3.2.3 Density of States (DOS) Profile

In order to understand the contributions of Ir, Ga, and Li atoms to the formation of the valence band (VB) and conduction band (CB) energies for the $LiGa_2Ir$ compound, as well as the possible hybridization and interactions between these atoms, we performed total and partial density of states (TDOS and PDOS, respectively) calculation. Figures 4 and 5 summarize the calculated TDOS and PDOS, respectively, of LiGa2 Ir structure with the presence and absence of SOC effect in the energy range between -11 eV and 7 eV with different XC approximations: PBE, PBE+U, and TB-mBJ. The Fermi level separates the VB from CB and is set at 0.0eV. The results show that the choice of XC approximation does not significantly affect the TDOS and PDOS profiles. However, significant SOC effects are seen in the TDOS profile at the energy range -4.5 eV to -2 eV, which may be due to relativistic effects, which play an important role in the accurate description of the electronic properties of compounds. The SOC effect corrects the total energy, thereby enhancing our understanding of the various characteristics of the compound. This effect becomes particularly pronounced when the inner shell electrons of heavy atoms, such as Ir, are close to the nucleus. Thus, the relativistic effects become crucial in this case because the SOC effect may enhance the kinetic energy of electrons [47, 48].

As can be seen from the TDOS graphs in Figs. 4(a)-4(c), in all XC approximations with and without SOC effects the $LiGa_2Ir$ compound has a metallic behavior confirming the results found in the band structure profile. We can understand the TDOS and PDOS profiles between the region -11 eV to 7 eV by dividing this interval into three different regions: the first region from -11 eV to -5 eV, the second region from -5 eV to 1 eV, and the third region from 1 eV to 7.0 eV.

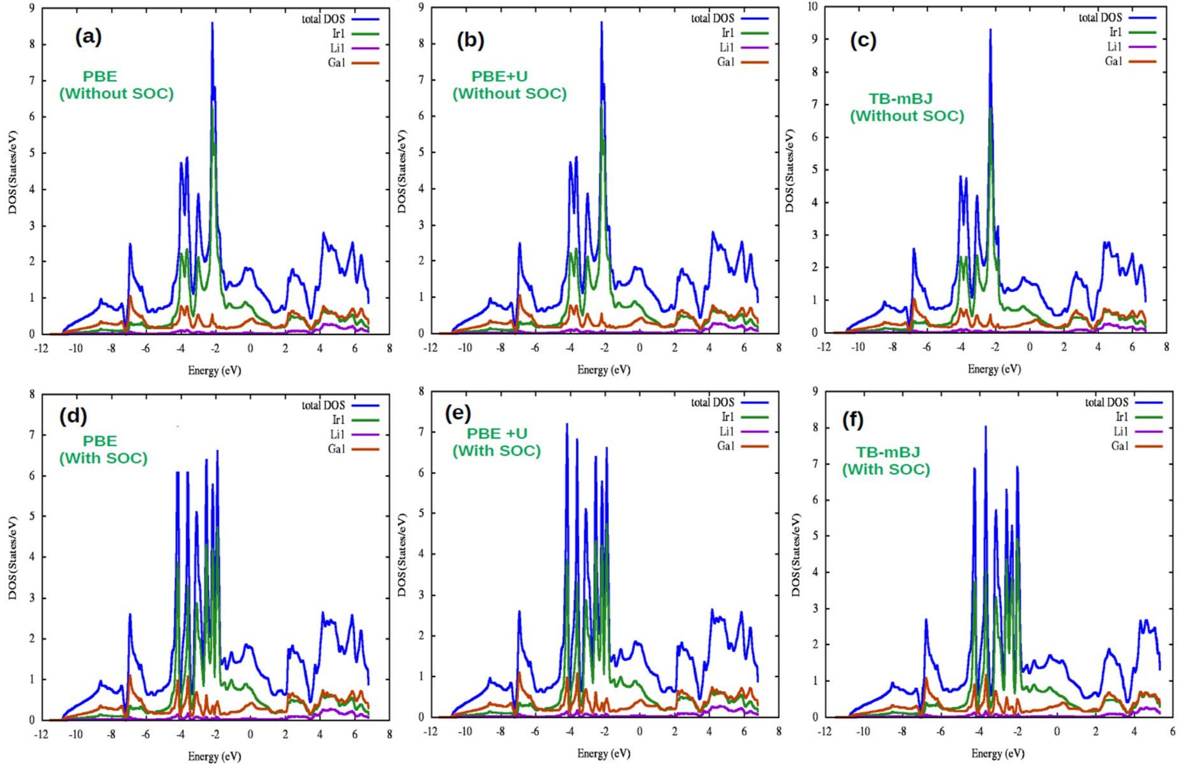

FIG. 4. Total DOS without SOC and with SOC for *LiGa$_2$Ir* using PBE, PBE+U, and TB-mBJ XC approximations.

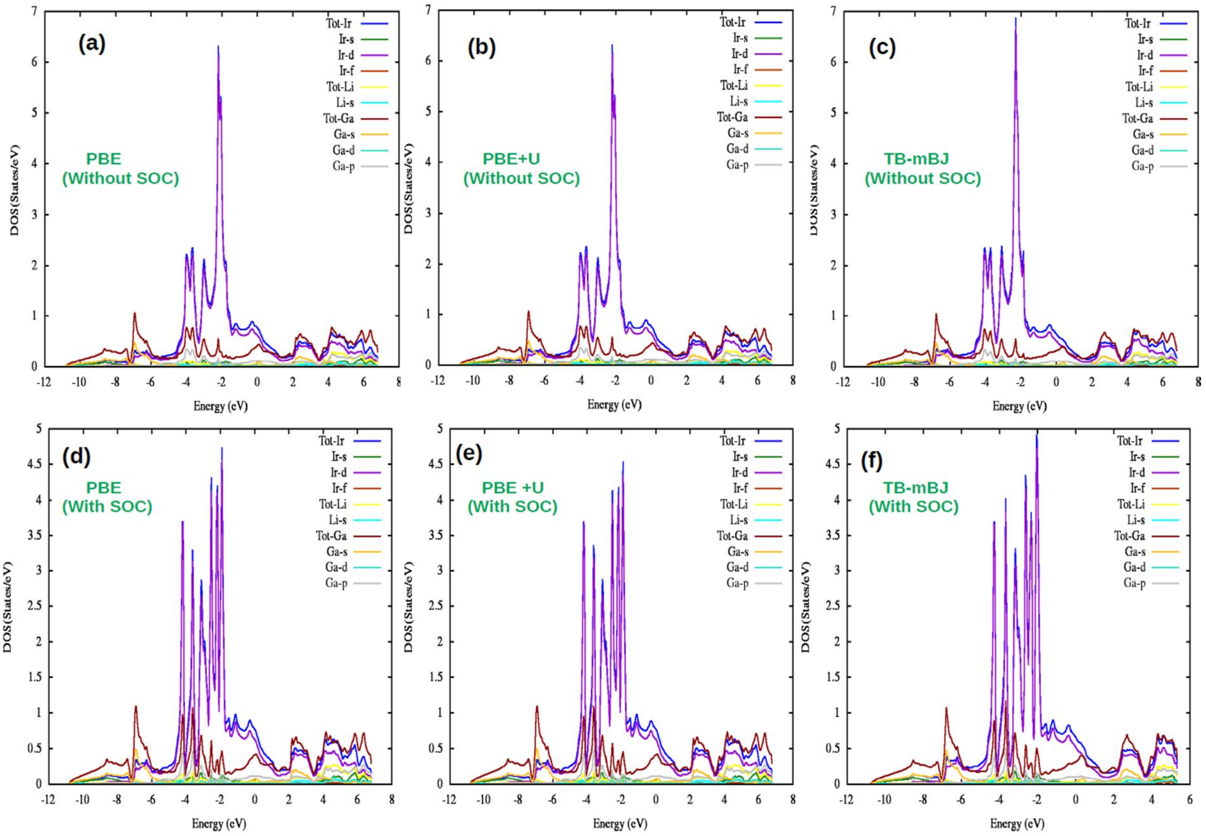

FIG. 5. Partial DOS without SOC and with SOC for *LiGa$_2$Ir* using PBE, PBE+U, and TB-mBJ XC approximations.

In the first region, deep inside the VB, across all XC approximations with and without SOC, it can be observed that the Ga atom (more precisely the Ga-s orbitals) predominantly contributes to the TDOS of the $LiGa_2Ir$ compound, with minimal contributions due to the Ir and Li atoms in this region.

In the second region (from -5 to 1 eV), strong peaks appeared clearly in the case of all XC approximations with and without SOC effect. The SOC effect is particularly noticeable here, especially with the TBmBJ approximation, as shown in Figs. 4(c), 4(f), 5(c), and 5(f), where there is an increase in the maximum values of the observed peaks. This region's maximum and high contribution comes from Ir-d orbitals for all XC approximations. There is also a smaller contribution from the Ga-p orbitals, suggesting that the hybridization between Ir-d and Ga-p orbitals is responsible for the observed TDOS profile, indicating strong interactions between these atoms. In contrast, the PDOS of the Li atom shows a weak contribution of Li orbitals.

In the CB's third region (from 1 eV to 7 eV), the TDOS and PDOS profiles change significantly, with a noticeable decrease in the intensity of the peaks compared to the second region in all cases of XC approximations with and without SOC. It can be observed that the major contribution is due to Ir and Ga atoms. The electronic states of Ir-d and Ga-p orbitals hybridize and contribute significantly to the TDOS profile in this region, indicating strong interactions between these atoms within the CB. The contribution from the Li atoms in the CB remains minimal.

4. Conclusion

In this work, the Li-based Heusler alloy $LiGa_2Ir$ was investigated using different XC in DFT calculations, both with and without the SOC effects. The stability, structural, and electronic properties were studied. The structure was found to be energetically stable, with a lattice parameter of a = 6.0927Å, which aligns well with experimental results. The electronic band structure and the DOS profile indicated a metallic behavior of $LiGa_2Ir$.

The results showed no significant differences between all XC approximations. However, it was observed that the SOC effects are much stronger for electronic states within the valence band (VB) at energies lower than the Fermi level (E_F), especially in the energy range of -4.5 eV to -2 eV. Understanding the $LiGa_2Ir$ and Heusler compounds' bonding structure was made possible by the PDOS profile. The findings revealed that Ir and Ga atoms make a significant impact, while Li atoms make a weaker contribution. This indicates a strong interaction between Ir and Ga atoms and their responsibility for the electronic behavior of the LiGa2 Ir compound.

Our findings suggest that the Li-based Heusler compound $LiGa_2Ir$ holds promise for further theoretical and experimental studies, particularly for applications in electronic devices such as metallic interconnectors.

References

[1] Graf, T., Felser, C., and Parkin, S.S., Prog. Solid State Chem., 39 (1) (2011) 1.

[2] Heusler, F., Starck, W., and Haupt, E., Verh. Dtsch. Phys. Ges, 5 (1903) 219.

[3] Belasri, A., Rached, D., Rached, H., Bourachid, I., Guermit, Y., and Caid, M., Eur. Phys. J. B, 94 (5) (2021) 1.

[4] Bainsla, L., Suresh, K., Nigam, A., Manivel Raja, M., Varaprasad, B.C.S., Takahashi, Y., and Hono, K., J. Appl. Phys., 116 (20) (2014) 203902.

[5] Wang, X., Cheng, Z., Wang, J., Wang, X.-L., and Liu, G., J. Mater. Chem. C, 4 (30) (2016) 7176.

[6] Klimczuk, T. et al., Phys. Rev. B, 85 (17) (2012) 174505.

[7] Guezmir, A., Rached, H., Bentouaf, A., Caid, M., Benkhettou, N., Rached, D., and Sidoumou, M., Comput. Condens. Matter, 28 (2021) e00573.

[8] Guermit, Y., Caid, M., Rached, D., Drief, M., Rekab-Djabri, H., Lantri, T., Rached, H., and Benkhettou, N., Int. J. Thermophys., 42 (6) (2021) 1.

[9] Huang, L., Zhang, Q., Yuan, B., Lai, X., Yan, X., and Ren, Z., Mater. Res. Bull., 76 (2016) 107.

[10] Elphick, K., Frost, W., Samiepour, M., Kubota, T., Takanashi, K., Sukegawa, H., Mitani, S., and Hirohata, A., Sci. Technol. Adv. Mater., 22 (1) (2021) 235.

[11] Cherif, H.S., Bentouaf, A., Bouyakoub, Z., Rached, H., and AÃ´rssa, B., J. Alloys Compd., 894 (2022) 162503.

[12] Berrahal, M., Bentouaf, A., Rached, H., Mebsout, R., and Aissa, B., Mater. Sci. Semicond. Process., 134 (2021) 106047.

[13] Bourachid, I., Rached, D., Rached, H., Bentouaf, A., Rached, Y., Caid, M., and Abidri, B., Appl. Phys. A, 128 (6) (2022) 1.

[14] Amudhavalli, A., Rajeswarapalanichamy, R., Iyakutti, K., and Kushwaha, A., Comput. Condens. Matter, 14 (2018) 55.

[15] Wang, C., Meyer, J., Teichert, N., Auge, A., Rausch, E., Balke, B., Hütten, A., Fecher, G.H., and Felser, C., J. Vac. Sci. Technol. B, 32 (2) (2014) 020802.

[16] Gottschall, T., Skokov, K.P., Benke, D., Gruner, M.E., and Gutfleisch, O., Phys. Rev. B, 93 (18) (2016) 184431.

[17] Yan, B. and de Visser, A., MRS Bull., 39 (10) (2014) 859.

[18] Bachaga, T., Zhang, J., Khitouni, M., and Sunol, J., Int. J. Adv. Manuf. Technol., 103 (5) (2019) 2761.

[19] Kojima, T., Kameoka, S., and Tsai, A.-P., Sci. Technol. Adv. Mater., 20 (1) (2019) 445.

[20] Benaisti, I., Guechi, N., Dehbaoui, M., and Boukaoud, A., preprint, Res. Sq., https://doi.org/10.21203/rs.3.rs-215061/v1.

[21] Damewood, L., Busemeyer, B., Shaughnessy, M., Fong, C., Yang, L., and Felser, C., Phys. Rev. B, 91 (6) (2015) 064409.

[22] Kandpal, H.C., Felser, C., and Seshadri, R., J. Phys. D: Appl. Phys., 39 (5) (2006) 776.

[23] Yadav, M.K. and Sanyal, B., J. Alloys Compd., 622 (2015) 388.

[24] Yao, W., Zhou, J., Zeng, D., Wan, H., Ruan, W., Liu, L., and Wen, Y., J. Magn. Magn. Mater., 503 (2020) 166642.

[25] Hadji, T., Khalfoun, H., Rached, H., and Azzouz-Rached, A., Comput. Condens. Matter, 27 (2021) e00557.

[26] Carnicom, E.M., Xie, W., Yang, Z., Górnicka, K., Kong, T., Klimczuk, T., and Cava, R.J., Chem. Mater., 31 (6) (2019) 2164.

[27] Hadji, T., Khalfoun, H., Rached, H., and Azzouz-Rached, A., Mater. Res. Bull., 143 (2021) 111461.

[28] Schwarz, K., Blaha, P., and Madsen, G.K., Comput. Phys. Commun., 147 (1-2) (2002) 71.

[29] Kandpal, H.C., Fecher, G.H., and Felser, C., J. Phys. D: Appl. Phys., 40 (6) (2007) 1507.

[30] Nakamura, K., Arita, R., Yoshimoto, Y., and Tsuneyuki, S., Phys. Rev. B, 74 (23) (2006) 235113.

[31] Liu, P., Khmelevskyi, S., Kim, B., Marsman, M., Li, D., Chen, X.-Q., Sarma, D., Kresse, G., and Franchini, C., arXiv preprint arXiv:1503.06753.

[32] Antonov, V., Bekenov, L., and Kukusta, D., Phys. Rev. B, 102 (19) (2020) 195134.

[33] Mazin, I., Jeschke, H.O., Foyevtsova, K., Valentí, R., and Khomskii, D., Phys. Rev. Lett., 109 (19) (2012) 197201.

[34] Górnicka, K., Kuderowicz, G., Winiarski, M.J., Wiendlocha, B., and Klimczuk, T., Sci. Rep., 11 (1) (2021) 1.

[35] Murnaghan, F.D., Proc. Natl. Acad. Sci. U.S.A., 30 (9) (1944) 244.

[36] Rached, H., Int. J. Quantum Chem., 121 (12) (2021) e26647.

[37] Elahmar, M.H., Rached, H., and Rached, D., Materials Chemistry and Physics 267 (2021) 124712.; Anisimov, V.I., Zaanen, J. and Andersen, O.K., Phys. Rev. B, 44 (1991) 943.

[38] Abada, A. and Marbouh, N., J. Supercond. Nov. Magn., 33 (3) (2020) 889.

[39] Dehghan, A. and Davatolhagh, S., J. Alloys Compd., 772 (2019) 132.

[40] Lone, I.U.N., Sirajuddeen, M., Khalid, S., and Raza, H.H., J. Supercond. Nov. Magn., 34 (5) (2021) 1523.

[41] Hadji, T., Khalfoun, H., Rached, H., Guermit, Y., Azzouz-Rached, A., and Rached, D., Eur. Phys. J. B, 93 (11) (2020) 1.

[42] Haid, S., Benstaali, W., Abbad, A., Bouadjemi, B., Bentata, S., and Aziz, Z., Mater. Sci. Eng. B, 245 (2019) 68.

[43] Kumar, A. et al., Optik, 249 (2022) 168250.

[44] Ahmadian, F., J. Alloys Compd., 576 (2013) 279.

[45] Rasool, M.N., Hussain, A., Javed, A., Khan, M.A., and Iqbal, F., Mater. Chem. Phys., 183 (2016) 524.

[46] Khandy, S.A. and Chai, J.-D., J. Magn. Magn. Mater., 487 (2019) 165289.

[47] Mellah, D.E. and Demmouche, K., Comput. Condens. Matter, 32 (2022) e00690.

[48] Verstraete, M.J., Torrent, M., Jollet, F.M.C., Zérah, G., and Gonze, X., Phys. Rev. B, 78 (2008) 045119.